Polarimetric radar observations during an orographic rain event

Michael Frech and Jörg Steinert

DWD, German Meteorological Service, Meteorologisches Observatorium Hohenpeißenberg, Albin-Schwaiger-Weg 10, D-82383 Hohenpeißenberg, Germany

DWD, German Meteorological Service, Frankfurter Str. 135, D-63067 Offenbach am Main, Germany

Correspondence to: Michael Frech
Michael.Frech@dwd.de

Abstract. An intense orographic precipitation event on 5th January 2013 is analyzed using a polarimetric C-Band radar situated North of the Alps. The radar is operated at the meteorological observatory Hohenpeißenberg (MHP, 1006 m above sea level) of the German Meteorological Service (DWD). The event lasted about 1.5 days and in total 44 mm precipitation was measured at Hohenpeißenberg. Detailed high resolution observation on the vertical structure of this event is obtained through a birdbath scan at 90° elevation which is part of the operational scanning. This scan is acquired every 5 minutes and provides meteorological profiles at high spatial resolution which are often not available in other radar networks. In the course of this event, the melting layer (ML) descends until the transition from rain into snow is observed at ground level. This transition from rain into snow is well documented by local weather observers and a present-weather sensor. The orographic precipitation event reveals mesoscale variability above the melting layer which can be attributed to a warm front. This variability manifests itself through substantially increased hydrometeor fall velocities. Radiosounding data indicate a layered structure in the thermodynamic field with increased moisture availability in relation to warm air advection. Rimed snow flakes and aggregation in a relatively warm environment lead to a signature in the radar data which is attributed to wet snow. The passage of the warm front leads to a substantial increase in rain rate at the surface. We use the newly implemented hydrometeor classification scheme "Hymec" to illustrate issues when relating radar products to local observations. For this, we employ data from the radar near Memmingen (MEM, 65 km west of MHP, 600 m, asl) which is part of DWD's operational radar network. The detection in location and timing of the ML agrees well with the Hohenpeißenberg radar data. Considering the size of the Memmingen radar sensing volume, the detected hydrometeor (HM) types are consistent for

measurements at or in a ML, even though surface observation indicate for example rain whereas the predominant HM is classified as wet snow. To better link the HM classification with the surface observation, either better thermodynamic input for Hymec or a statistical correction of the HM classification similar to a model output statistics (MOS) approach may be needed.

1 Introduction

Orographic rain events in the vicinity of the Alps can last a couple of days and often have the potential to produce flooding conditions. The Alps represent a natural barrier for advected moist air which either initiates or intensifies the upstream precipitation process (Houze and Medina, 2005). The precipitation events are often persistent and depending on the season, transitions from rain into snow caused by diabatic cooling of the associated airmass can be observed (Lackmann et al., 2002). From an operational point of view, precipitation amount and hydrometeor type are important parameters which are needed to issue proper warnings to the public. For example, correct precipitation amounts are important for flood management, and hydrometeor classification is an important parameter for traffic management. Here, modern polarimetric radar systems are the only systems which are able to provide spatial information about the spatial variability of precipitation intensity and the corresponding hydrometeor type (Scharfenberg et al, 2005).

The principal physical processes of precipitation are well known but with the availability of new technology often a closer and also new look into the precipitation process becomes possible, especially when new methods and algorithms such as a hydrometeor classification move from the

research world to the operational world of a weather service, simply because more observations become available.

The local intensification of precipitation over mountain ranges during the passage of mid latitude winter storms has been studied in detail in the work of Houze and Medina (2005). There, data from extensive field campaigns reveal the dynamic and microphysical processes in particular upstream of a mountain ridge. Depending on the stability of the atmospheric flow, either turbulent mixing or vertical transport induced by gravity waves (triggered by orography) can produce pockets of higher liquid water content which intensify riming and growth of ice particles above the melting layer so that they eventually cause a polarimetric radar signature typical for Graupel with reflectivity values on the order of 40 dBZ. In fact, coinciding airborne in-situ measurements identified Graupel particles.

In this paper we analyze an orographic precipitation event in Southern Germany which occurred on the 5th January 2013. The analysis focuses on the mesoscale variability of the precipitation event. The observed variability has some similarities to the measurement campaigns discussed in Houze and Medina, (2005). However, some of the details are different, which will be elaborated in this work. Here, we study the spatial and temporal variability of the precipitation field using radar data and surface observations. The surface observations are taken at the meteorological observatory Hohenpeißenberg which is located on a mountain in southern Bavaria, about 1000 m above sea level. South of the observatory, the Alpine mountain ridge is about 15 km away (Figure 1). Aside from standard meteorological surface measurements, disdrometer data are available. Furthermore, we can make use of observations from experienced weather observers. The Hohenpeißenberg site is also hosting the dualpol research radar of the German Meteorological Service (DWD). Radar data from a scan at 90° elevation and data from another operational radar about 65 km away are used to investigate this event. The scan at 90° elevation, commonly refered to a birdbath scan, operationally becomes more and more available from national weather radar networks because polarimetric radar system are typically introduced now. Then, if possible, a birdbath scan is the prime choice to calibrate differential moments (see next section). So far the meteorological information available from this scan is usually not exploited. In this work we investigate an intense precipitation event and highlight the additional value of the birdbath scan data in relation to the understanding of the overall meteorological situation.

What we refer to a mesoscale event is characterized by large hydrometeor fall velocities which are usually not expected above the melting layer. The large fall velocities are persistent for about one hour and coincide with increased surface precipitation rates. This can be inferred with a combination of radar and surface data. In addition, results from the a hydrometeor classification scheme are qualitatively compared to the local observation. One of the reasons to intro-
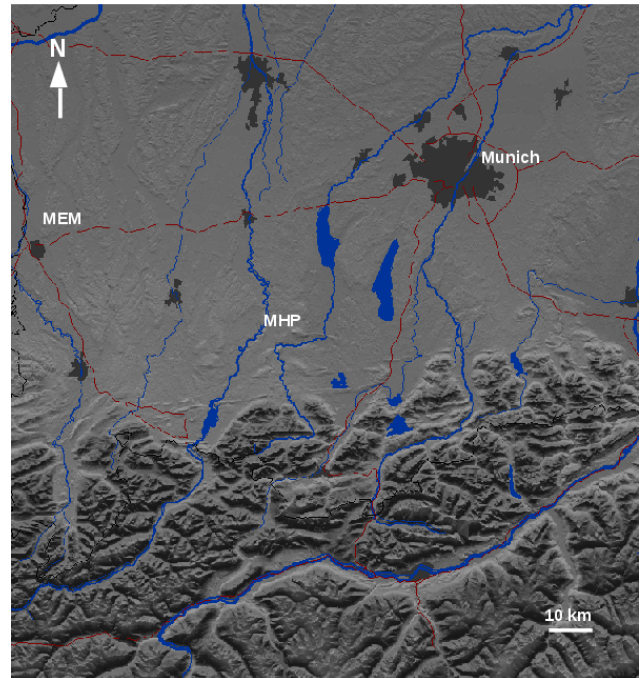
Fig. 1. Geographic location of the observatory Hohenpeißenberg (MHP, 1000 m asl) and the radar Memmingen (MEM). The surrounding orography is also shown.

duce polarimetric radars is the expectation of an improved and more detailed hydrometeor classification. Quantitative precipitation estimators using polarimetric radar data as input are expected to perform better than the classic Z/R relationships (Ryzhkov et al., 2005), and in particular they are expected to benefit from hydrometeor classification. Therefore, understanding this observation will be also one element in improving and optimizing the surface precipitation rate estimates based on polarimetric radar data.

In this contribution we first introduce the radar data. Then a brief overview on the methodology of the hydrometeor classification is given. This is followed by an introduction of the synoptic setting of this orographic precipitation event. Then we analyze the features of the precipitation event using radar data, surface observations and the results from the hydrometeor classification. The main findings are summarized in the last section.

2   Radar data

The new generation of radar systems of the German weather radar network, EEC's DWSR5001C/SDP, is fully polarized. The systems are run in a hybrid (STAR) mode transmitting simultaneously in horizontal and vertical polarization (see Frech et al., 2013 for some more technical details of the new system). A magnetron based transmitter generates pulses

with 500 kW peak power. The operational pulse widths are 0.4 and 0.8 μs. The antenna has a diameter of 4.3 m, and the antenna gain is better than 45 dBi. The resulting 3dB beam width is $1°$. The antenna is protected by a quasi-random panel radome, which is optimized for dualpol applications. The radar system has an antenna mounted receiver. There, the received analog signals are digitized, and the in phase and quadrature phase (IQ) data are transmitted through an optical rotary joint to the linux-based signal processor Enigma3p by GAMIC, where the radar moments are computed in real-time.

The scan strategy guarantees an update rate of 5 minutes. It comprises a terrain following scan (the so called precipitation scan), a 5-minute volume with 10 sweeps at 10 different elevations and a "birdbath" scan at $90°$ elevation. Latter scan is part of the scan strategy because of the necessity to calibrate differential moments such as the differential reflectivity ZDR. The differential reflectivity of falling hydrometeors must be 0 dB when looking vertically upward. Hardware specific offsets can be derived and monitored using this scan. This scan can also be used to monitor the absolute calibration of the radar system (Frech, 2013). Aside from this, the birdbath scan can be viewed as a profiler scan and is as such a very interesting scan from a meteorological point of view. So far this scan is not used operationally for this purpose. The birdbath scan provides a high resolution look of the precipitation process above the radar site. This will be highlighted in this paper. The radar systems are operated with a rangebin resolution of 250 m (terrain following scan), 1000 m (volume scan) and 25 m (birdbath scan).

In this work we use data from the research radar at DWD's meteorological observatory Hohenpeißenberg (MHP) and the Memmingen radar (MEM), latter is part of DWD's operational radar network. Both systems are identical in hardware. The configuration of the research radar is comparable to the Memmingen system. In general, the research system does not provide operational data.

The introduction of the new dual-polarization radar system was accompanied by a project called "Radarmaßnahmen". This in-house DWD project covers the development of radar data processing algorithms, e.g. for quality assurance, hydrometeor classification and quantitative precipitation estimation and the development of a software framework which is called "POLARA" (Polarimetric Radar Algorithms), Rathmann and Mott (2012). The aforementioned algorithms within the POLARA framework are operational. The users within DWD are currently verifying the new products such as the hydrometeor classification.

3 Hydrometeor classification

Polarimetric measurements of a dual-polarization radar allows the classification of the hydrometeor type (HM). Commonly, fuzzy-logic classification schemes are employed to determine the most probable HM type (Straka et al., 2000, Keenan, 2003, Lim et al., 2005, Park et al., 2009, Al-Sakka et al., 2013). The verification of a classification scheme is typically done with test data sets, where hydrometeor types are known (Al-Sakka et al., 2013). Radar derived classification results can be related to surface observation by using model predicted thermodynamic profiles (Schuur et al., 2012). The biggest challenge is a situation with mixed precipitation where a validation is usually difficult. At DWD, we implemented a fuzzy logic hydrometeor classification algorithm (Hymec) which follows Park et al.(2009). The fuzzy logic method itself is based on trapezoidal membership functions (MBF) for each pair of input parameter and hydrometeor class. For the parameterization of the MBF for radar input the values of Park et al. (2009) are used. The winner class of the fuzzy logic is estimated with the maximum method related to the class probability. The winner class must exceed a threshold (35% probability for the HM classes, and 65% probability for the ML class). If the class probability is below this threshold, the class is tagged as 'not classified' (NC).

The choice of hydrometeor classes in Hymec is based on a user survey among the forecasters. For them the light rain class (drizzle) deemed to be a especially important class. The following classes are covered in Hymec: drizzle, raindrops, big drops, wet snowflakes, dry snowflakes, ice crystals, graupel, heavy rain or hail stones and hail stones. In addition, the melting layer (ML; bright band) represents a class on its own. In the Hymec algorithm chain the melting layer detection is done prior the hydrometeor classification. We use the ML detection as an additional source of information which is offered to the user to interpret the meteorological situation. Algorithms like the quantitative precipitation estimation (QPE) use the knowledge of the ML location and the type of hydrometeor to utilize appropriate precipitation estimation algorithms.

The input data for Hymec consists of radar data and model output data from the weather forecast model COSMO-DE (Baldauf et al., 2014). The radar moments used are the reflectivity in horizontal polarization, Zh, the differential reflectivity ZDR, the specific differential phase KDP and the co-polarization correlation coefficient ρ_{hv}. The radar moments have passed a quality control chain, where especially clutter segments and other non-meteorological artefacts in the radar data like spokes and rings are removed or corrected (Werner and Steinert, 2012). Zh and ZDR are corrected for attenuation based on the self-consistency principle (Bringi and Chandrasekar, 2001). As the attenuation correction algorithm needs homogeneous (related to hydrometeor class) ray segments, the results of a first Hymec run is used as input (Figure 2). The COSMO-DE model temperature is used to separate between liquid and solid hydrometeor types, in order to separate snow flakes and small raindrops which give similar radar signatures. From the model we use the height of the $0\,°C$-isotherm, HZEROCL, and the snowfall altitude SNOWLMT. Furthermore, a history of the detected ML based on the anal-
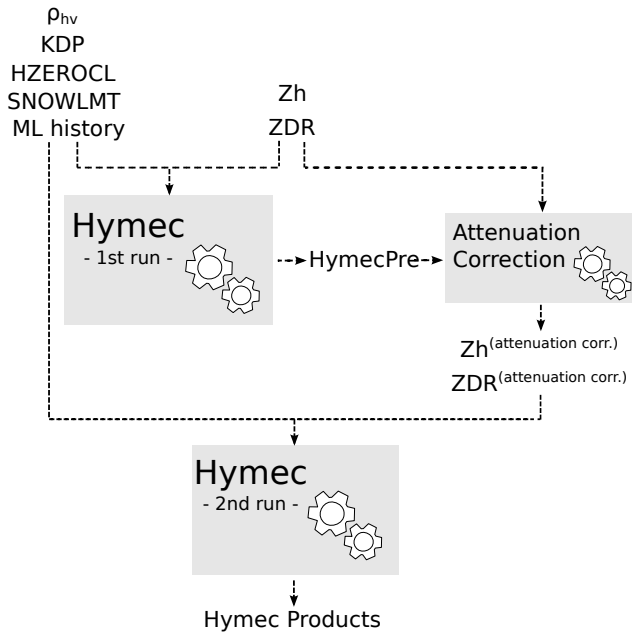
Fig. 2. The two-step Hymec algorithm run. The first Hymec run provides the attenuation corrected Zh and ZDR. The dashed lines denote the data paths of the algorithm.

ysis of the full radar volume is created (Figure 3). This im-
proves the classification results especially at lower elevations
where the detection of a ML is difficult (Giangrande et al., 2008).

Hymec is implemented as a two-stage algorithm sequence. A sketch of the embedded classification processing chain is shown in Figure 2. An initial HM classification is performed prior the attenuation correction. In the subsequent HM classification the attenuation corrected moments are used to come up with the final HM classification (Steinert et al., 2013). Furthermore, the ML history is updated so that it can be used for the next run.

4 The synoptic situation

An intense orographic precipitation event was observed north of the Alps on the 5th January 2013. The event lasted about 1.5 days and in total 44 mm precipitation was measured at Hohenpeißenberg. Synoptically, Germany was located at the forefront stationary longwave ridge which extended from the Iberian Peninsula up to the British Isles (Figure 4). Embedded in the upper air-flow from north a warm front caused the intense and persistent orographic rain event especially in South-Eastern Bavaria. Based on Figure 4, the warm front is located in southern Bavaria at around 12 UTC.

The operational 12 UTC radiosonde sounding from Munich (about 50 km north from Hohenpeißenberg) provides further information about the vertical thermodynamic and
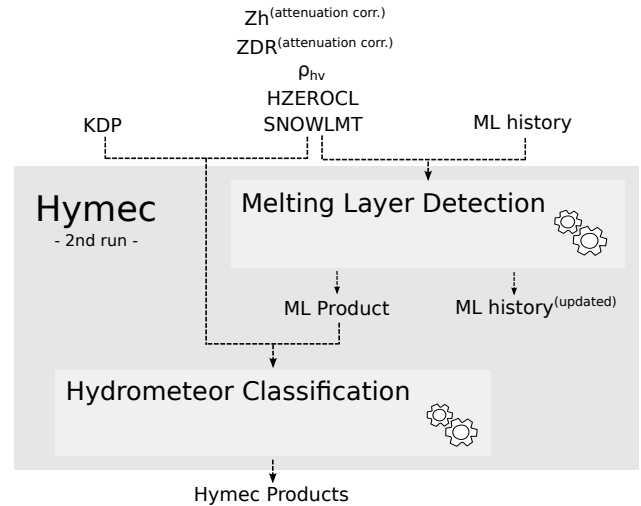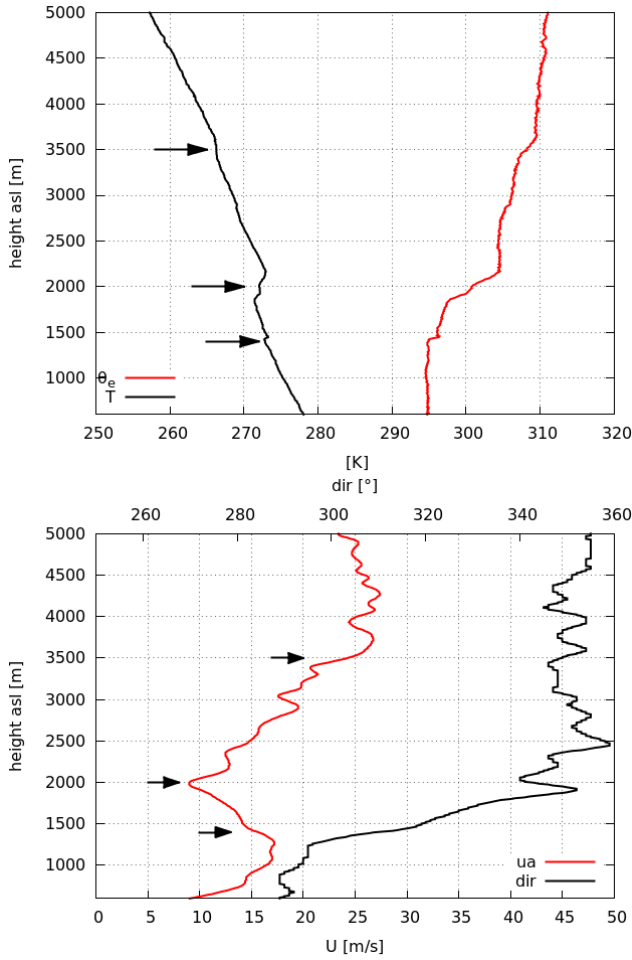

Fig. 3. The inner structure of the 2nd run of the Hymec algorithm (see Figure 2) which includes the melting layer detection and update, and the hydrometeor classification. The Hymec processing is done for every PPI sweep and for each radar station separately.
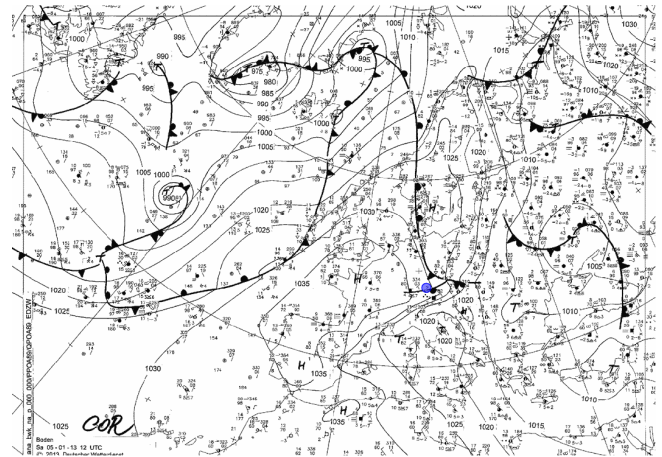
Fig. 4. DWD's synoptic analysis 5th January 2013, 12 UTC. The approximate location of the Hohenpeißenberg observatory is marked with a blue dot.

dynamic structure of this event (Figure 5). Here we use the high resolution data set with about 10 m resolution in the vertical. The veering of the wind vector with height in a layer between about 1200 and 2000 m is an indication of warm air advection. There the winds turn from north-west to a wind direction from north. Below 1200 m and above 2000 m, the wind direction is nearly constant with height. The thermodynamic profiles up to a height of 5000 m show a four layer structure which is visible in the temperature profile. There are temperature inversions near 1400 m, 2000 m and 3500 m. The approximate locations are marked in Figure 5. The layer between 1400 m and 2000 m in the wind profile corresponds
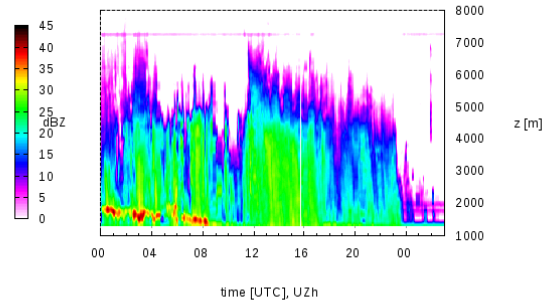
Fig. 6. Time-height plot of UZh based on the birdbath scan which is available every 5 minutes. Data are from 5.1.2013 until 6.1.2013 in the morning, radar MHP.

Fig. 5. Munich radiosonde data 5th January 2013, 12 UTC: Temperature T and the equivalent potential temperature Θ_e (upper panel) and wind speed and direction,lower panel.

well to the significant warm air advection. Relative warm and moist air is advected over a cooler airmass below. The four layer structure can also be seen in the equivalent potential temperature profile Θ_e. The lowest layer is neutral stratified, the other layers have neutral and slightly stable stratified sections with respect to Θ_e. Based on the sounding, the 0°C - level is near 1340 m.

5 The orographic precipitation event: surface and radar observations at Hohenpeißenberg

We first analyze data from the birdbath scan in order to highlight the temporal evolution of this orographic precipitation event in detail. During Saturday (5.1.2013) a transition from rain into snow was observed. The Hohenpeißenberg weather observer noted sleet starting 14:40 UTC and pure snow fall beginning 16:45 UTC. Figure 6 is a time-height plot of the unfiltered reflectivity factor UZh starting

00:00 UTC, 5.1.2013, ending 3:00 UTC 6.1.2013. Unfiltered UZh means that no clutter filter has been applied. Only data above approximately 600 m above the radar site are shown, which approximately corresponds to the far field of the radar antenna. Meaningful data is expected from this range on. From Figure 6 we see the initial location of the melting layer (large UZh values) which gradually descends before it is below 1600 m at about 9:00 UTC. The corresponding Doppler velocity is shown in Figure 7. The velocity shown here can be considered to be the effective terminal fall velocity of the hydrometeors. Effective, because updrafts and downdrafts may be both present depending on the meteorological situation. In the case of a stratiform rain event (a typical feature is the presence of a melting layer), the vertical velocity is expected on the scale of cm/s above the ML. The location of the melting layer is again nicely visible in the Doppler data. As soon there is a transition from snow into rain, terminal fall velocities increase up to 3-8 m/s, depending on the resulting drop sizes. Above the ML velocities are usually on the order of cm/s or less, indicative of snow (Szyrmer and Zawdazki, 2010). These distinct features cannot be separated out from operational Doppler data at low elevations. Here, the Doppler data also reveal the mesoscale feature which will be investigated below. We find fall velocities on the order of -3 m/s between approximately 11 and 12 UTC which cannot be attributed to dry snow. Based on the fall velocity magnitude is characteristic for wet snow or Graupel (Yuter et al., 2006). Note that the melting layer is below this mesoscale feature. We call this a mesoscale feature because of the large spatial (horizontal) length scale of this feature which is on the order of 25 km. This is estimated as $L = U \cdot T$ with $U = 7$ m/s and the duration of the event $T = 1$ hr. The horizontal velocity estimate U is based on surface wind measurements. The region with large fall velocities reaches up to 4 km asl.
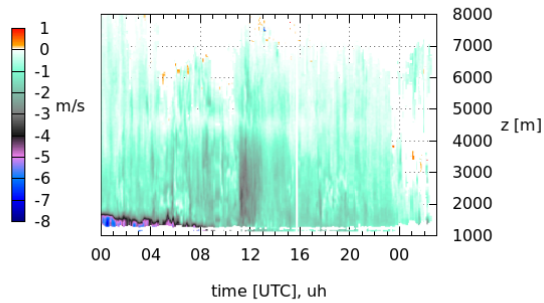
Fig. 7. Time-height plot of Doppler velocity based on the birdbath scan which is available every 5 minutes. Data are from 5.1.2013 until 6.1.2013 in the morning, radar MHP. The data represents the effective terminal fall velocity of the hydrometeors (negative towards the surface).

The time-averaged profiles for specific time intervals (which roughly exhibit homogeneous characteristics) are shown in Figure 8. The mean profiles are supposed to quantify the distinct difference between the time intervals. The most apparent difference is highlighted by the fall velocity. Fall velocities on the order of 3 m/s found during the mesoscale event can only be seen below the bright band during the early morning hours of the 5th January. The full scale of the melting layer is not revealed here as it is below the first radar range bin that can evaluated. We see the decrease of ρ_{hv} which has not reached its minimum value (here 0.94). ρ_{hv} values as low as 0.8 can be found in the melting layer. The peak of UZh is at a higher altitude than the minimum ρ_{hv}. A reduction of ρ_{hv} is expected if there is a large variety of hydrometeors present in the sampling volume. Smaller ρ_{hv} points to a rain / snow mixture. As soon as all snow is melted, ρ_{hv} is close to one again (see e.g. the profile after the "event" in Figure 8). The largest UZh values are expected where the snow just starts to melt and snow flakes become coated with a water layer. The width of the melting layer can be up to 700 m as it was observed in the stratiform part of a mesoscale convective system (Frech, 2013). Based on the bright band observations in the early morning hours, the width of the melting layer appears to be on the order of 500 m. During the mesoscale event, reflectivity factors on the order of 22 dBZ are found. After the passage we find actually an increase up to 25 dBZ which however does not have a correspondence to the fall velocities (Figure 8). This appears indicative of small wet snow flakes. A substantial decrease of UZh to below 20 dBZ can be noted at about 17 UTC (Figure 6) when surface observations report snowfall. Lower reflectivity factors suggest dry snow flakes. Note that the small

ρ_{hv} values at higher elevations correspond to Zh values lower than 5 dBZ or less. Small ρ_{hv} values may occur because we are at the top of the precipitating cloud where the temporal variability of the scattering particles may be large and SNR is small.

With the help of the surface observations which indicate the transition into snow at 16:45 UTC, we can argue that the surface measurements between about 9 UTC and 16:45 UTC are taken in the melting layer before we see the transition into snow. This needs to be kept in mind in the following analysis.

We now investigate the corresponding surface observations. The time series of wind measurements based on an ultrasonic anemometer is shown in Figure 9.

The whole event is characterized by a constant wind direction. Wind speeds are on the order of 7 m/s, decreasing to about 5 m/s at about 14 UTC. Between 11 and 12 UTC there is no apparent change in wind speed and direction during the passage of the mesoscale feature observed in the radar data. In the case of a dynamic effect we may expect some evidence of horizontal divergence or convergence in the wind data. This can be a drop in wind speed or a change in wind direction. What we find however is a drop in surface pressure by about 1 hPa which is indicative of a dynamic effect even though it is not directly visible in the wind data. Possibly, lifting processes, latent heat release and the capture of water droplets by snow lead to riming and generation of graupel or wet snow (Fabry and Zawadzki, 1995). Note, rain was still observed at the surface during the passage of this mesoscale event.

The corresponding observations of a Thies optical disdrometer are shown in Figure 11. The optical disdrometer measures the hydrometeor size and fall speeds. Aside from precipitation rates a classification scheme based on the hydrometer sizes and fall speeds, together with a temperature measurement provides a diagnostic of the hydrometeor type. The principal ideas and the caveats of the measurement principle are discussed in e.g. Friedrich et al. (2013). During the passage of the mesoscale event there is an intensification of precipitation rate with an increase from 1 mm/h to on average 2 mm/h (Figure 12). The relative contribution of the solid and liquid phase to the absolute precipitation rate does not reveal a link to the mesoscale precipitation event aloft. Nicely visible is the transition to snow fall in disdrometer data which corresponds very well to the observation of the weather observer (the ratio between solid QPE and total QPE becomes one). Timing and the transition corresponding to the sleet observation are well diagnosed by the disdrometer. Before that the liquid phase contribution is larger on average. Some of the variability of the ratio is related to small precipitation rates and the variability of the precipitation process itself where small variations in precipitation rates can lead to large fluctuations of the resulting precipitation ratio (Figure 11).

But now we are coming back to the observed surface pressure drop. The 12 UTC surface analysis (Figure 4) indicates
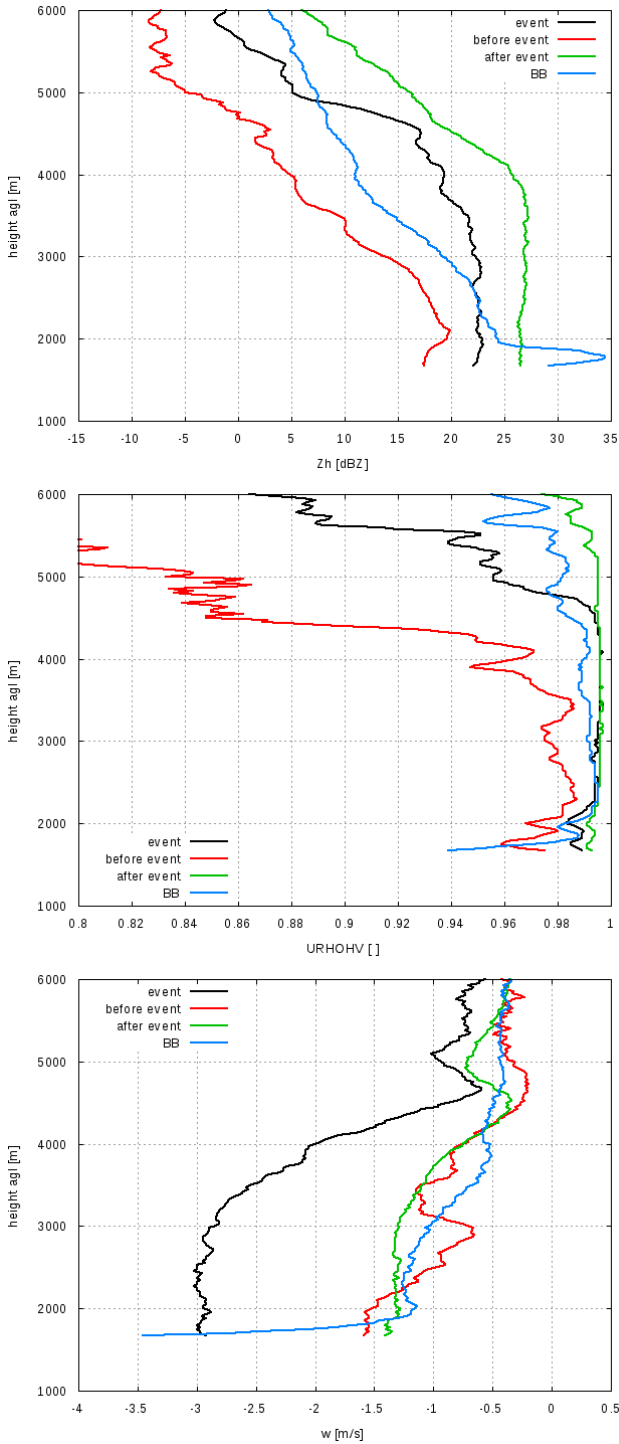
Fig. 8. Time averaged profiles of UZh (upper panel), ρ_{hv} (middle panel) and fall velocity (lower panel) for specific time intervals: before the event (10 - 11 UTC), the event itself (11:10 - 11:40 UTC), and after the event (13:00 - 14:00 UTC). In addition we show a mean profile when the bright band is clearly visible (0:00 - 0:50 UTC).
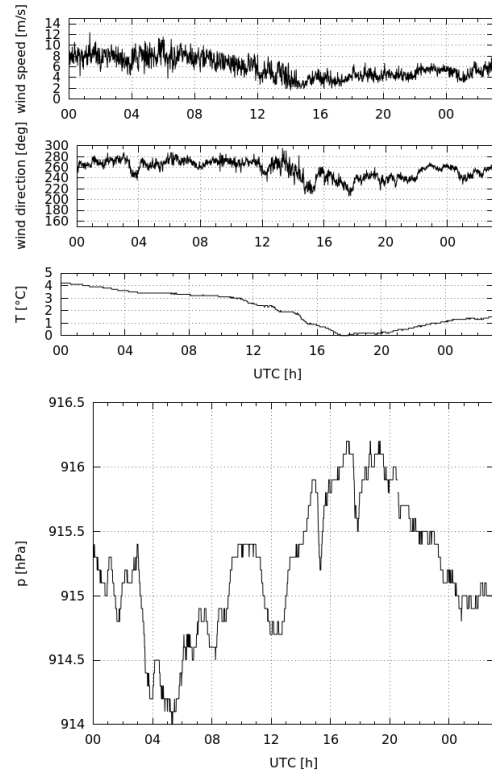
Fig. 9. Time series of wind speed, wind direction (measured by a ultrasonic anemometer) and temperature (upper panel). Measurements are taken at the Hohenpeißenberg observatory. The corresponding surface pressure (hPa) is shown in the lower panel. Data start at 0 UTC, 5th January 2013 and end at 3 UTC, 6th January 2013.

a warm front during time where we observe the mesoscale scale variability in the radar data. Furthermore, the sounding data indicates the advection of relative moist and warm air aloft (at heights larger 1400 m). Note that the temperature is below 0°C: based on the sounding we have −1°C at 1600 m and −9°C at 4000 m. This suggests that the mesoscale variability relates to the passage of the warm front from north to south. As such the radar measurements represent a cross section through this front when it is passing the site from north to south. So the combination of frontal activity, increased moisture availability leads to enhanced riming of snow and aggregation. The large fall velocity relates to wet snow. The aggregation process is expected to be further enhanced due to the orography where the airmass is forced to ascend. In addition, local turbulent mixing may play a role in supporting the aggregation process, because the static stratification (near neutral to slightly stable with respect to Θ_e) and the wind shear between 1600 and 4000 m (see Figure 5) are favorable to support turbulence locally. This can be expected based on the corresponding profile of the gradient Richardson number (following the approach of Houze and Medina, 2005) which has been computed using the sounding data (Figure 10). The
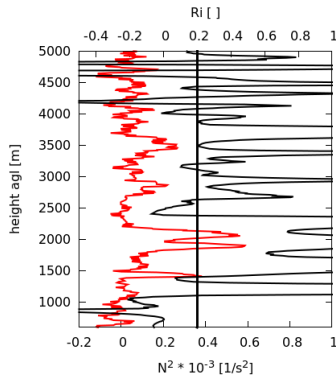
Fig. 10. The profiles of the dimensionless gradient Richardson number Ri and the squared Brunt-Vaisala frequency N^2 $[1/s^2]$ (red curve). Profiles are based on the Munich radiosonde data. Also shown is the critical Richardson number of 0.2. The flow supports turbulence for $Ri < 0.2$. Below 1000 m, the atmospheric conditions are favorable for turbulence. Layers potentially supporting turbulence are found between 1000 and 4000 m.

Fig. 11. Raw and smoothed (in blue) time series of precipitation rate (mm/h) based on the Thies optical disdrometer (lower panel). The relative contribution of the liquid and solid phase precipitation to the total QPE (defined as the ratio of e.g liquid QPE divided by the sum of liquid and solid QPE), upper panel. The ratio is only computed for precipitation rates larger then 0.1 mm. The resulting time series is then smoothed with a spline fit. Data shown begin at 0 UTC, 5th January 2013.
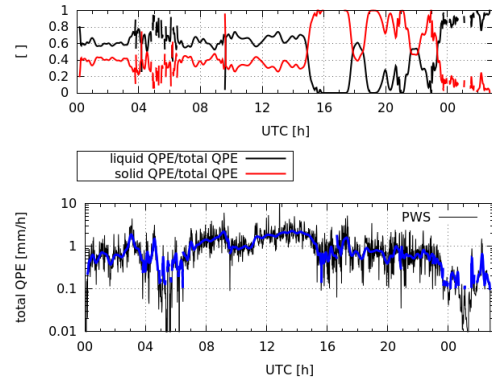
gradient Richardson is the ratio of the buoyancy production term and shear production term of turbulence which is related to the *local* gradients of the mean flow. Turbulence can be expected with a gradient Richardson number smaller than 0.2.
455 Further enhancement of turbulent mixing may be expected in the warm front itself.

After the passage of the warm front, reflectivity factors further increase (Figure 8), but fall velocities drop significantly (< 1.5 m/s). These fall velocity are related to large aggre-
460 gated snow flakes (Szyrmer and Zawadzki, 2010, Ryzhkov et al., 1998) in a cooler environment. Note, that this warm front is embedded in a continuous precipitation event.
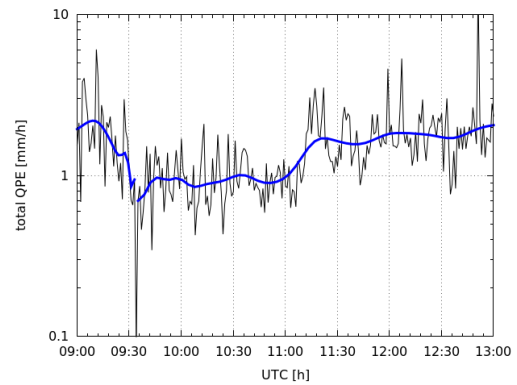
We have focused here on the event which is interpreted as the signature of a warm front. It has to be noted, that there
465 are pockets of increased fall velocities present throughout the day, but on a shorter time and length scale. They are likely to be in relation to the warm front and the associated airmass characteristics. As an example we refer to the signature at about 8:30 UTC in Figure 7 which is also reaching up to
470 4000 m.

Fig. 12. Raw and smoothed (in blue) time series of precipitation rate (mm/h) based on the Thies optical disdrometer. Zoom in to the time period with the passage of the mesoscale event (between about 11:00 and 12:00 UTC). Data shown are from 5th January 2013.

6 Memmingen radar observations and hydrometeor classification

In the previous section we have analyzed surface data and bird bath radar data at Hohenpeißenberg. Radar data show
475 distinct mesoscale features which result in an increase in surface rain rate which can be related to a warm front. The whole precipitation event is an example where the ML, initially nicely visible in the radar data (see early morning hours in Figure 6), descends during the day. For a couple of hours
480 the Hohenpeißenberg mountain top is actually within the ML before the surface observations indicate the transition into

snow. We investigate the hydrometeor classification (HM) based on the Memmingen radar which is located 65 km West of Hohenpeißenberg. Aside from the HM classification we
485 investigate whether there are indications in the spatial HM variations which can be related to the observations of the birdbath scan. Before we go into detail it is necessary to point out the length and time scales involved when using in-situ measurements and radar measurements. With the main beam
490 width of $1°$, the radar pulse at a distance of 65 km has a width of about 1.1 km. The bottom of the radar pulse at an elevation of $0.5°$ is at about 960 m as which corresponds approximately to the height of the Hohenpeißenberg, the top of the pulse volume is near 2000 m. Recall that the range resolution
495 is 1 km. The instantaneous radar measurement of this pulse
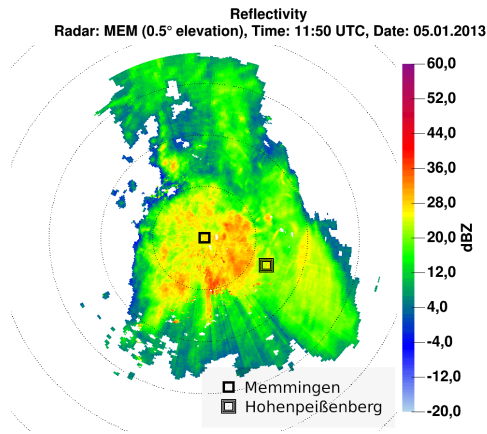
Fig. 13. PPI of attenuation corrected Zh at an elevation of 0.5° for the Memmingen Radar at 11:50 UTC. The location of Hohenpeißenberg is indicated.
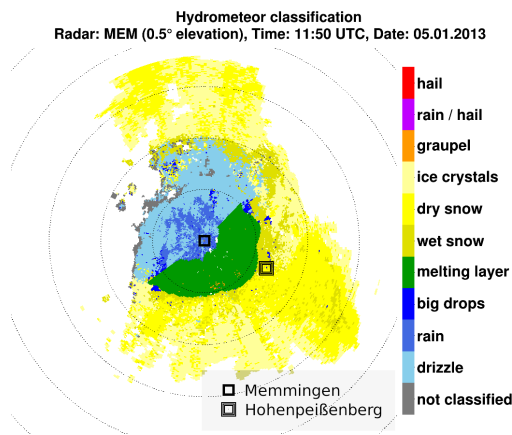
Fig. 14. PPI of the hydrometeor classification at an elevation of 0.5° for the Memmingen Radar at 11:50 UTC. The location of Hohenpeißenberg is indicated.

volume is compared to an in-situ instrument which integrates over time (1 minute). A perfect correspondence may only be expected if the meteorological phenomena is homogeneous in time and space for at least the time and length scales involved here. It is obvious that this will be only approximately the case here.

A PPI of the attenuation corrected Zh at the lowest elevation is shown in Figure 13. It is taken at 11:50 UTC while the front is passing the Hohenpeißenberg. The corresponding HM classification results are shown in Figure 14. Based on the HM classification there is a gradient in snowfall altitude from North-West to South-East. This is highlighted by the fact that there is no circular melting layer "ring" around the radar. Instead, we find only a ring segment. This indicates a diabatic cooling effect associated with the synoptic scale warm front. During the persistent precipitation near the Alps, melting snow falling into the relatively warm airmass
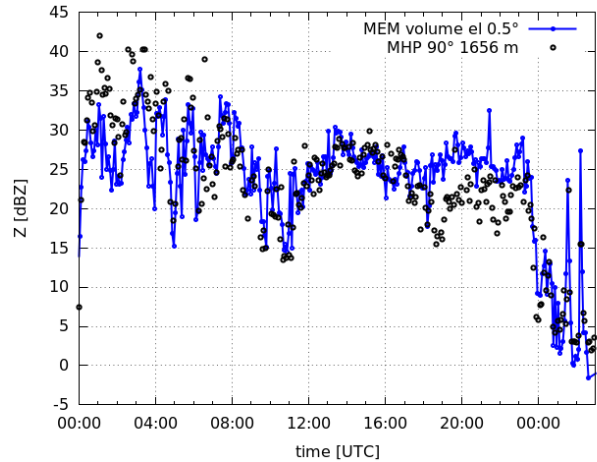

Fig. 15. Time series of the reflectivity factor from the first far field rangebin (about 650 m above the site) of the birdbath scan at MHP and the the MHP rangebin from 0.5° elevation of the MEM radar. Data are from 5th January 2013, 0:00 UTC until 6th January 2013, 3:00 UTC.
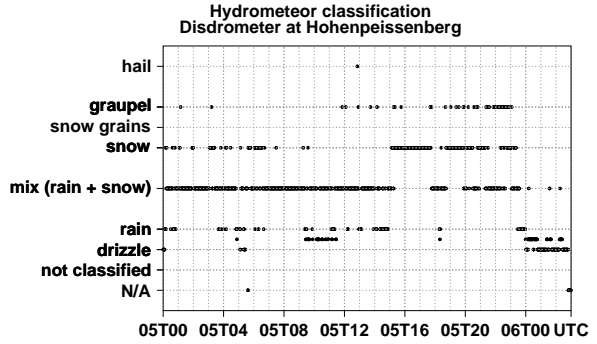
is causing diabatic cooling which leads to the continuous decrease of snowfall altitude (e.g. Lackmann et al., 2002, and references therein). The HM classification around the Hohenpeißenberg site predominantly shows wet snow associated with reflectivity factors on the order of 25 dBZ, consistent with the observation of the birdbath scan (Figure 14). There are spots indicating rain with big drops which correspond to regions with enhanced Zh (Figure 13). The Hohenpeißenberg weather observer still report rain during this time period. Obviously the scattering characteristics in the pulse volume is predominantly governed by the wet snow aloft, and not by the layer with rain close to the surface.

Time series of the reflectivity factor from the first far field rangebin of the birdbath scan at MHP and the MHP rangebin from 0.5° elevation of the MEM radar are shown in Figure 15. More or less large differences are found during times with vertical variations of HM type. This is due to the significantly larger sampling volume of the MEM radar sensing volume which becomes apparent in the morning hours when the ML is present. There, MHP reflectivity values represent measurements in the ML whereas at the MEM sensing volume only sees a combination of ML, rain and snow with a smaller effective reflectivity value. If precipitation is relatively homogeneous in space, the agreement is much better. This is the case for example between 09:00 and 17:00 UTC.
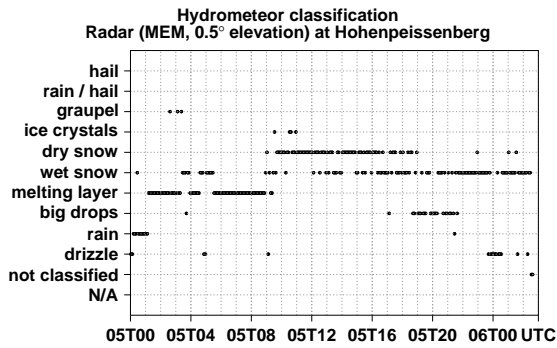
We will now compare a time series of HM classification based on the Memmingen radar with the standard HM classification of the optical disdrometer on the Hohenpeißenberg. The radar HM results are shown in Figure 16 where the classification is shown as a time-height series based on volume data available every five minutes.
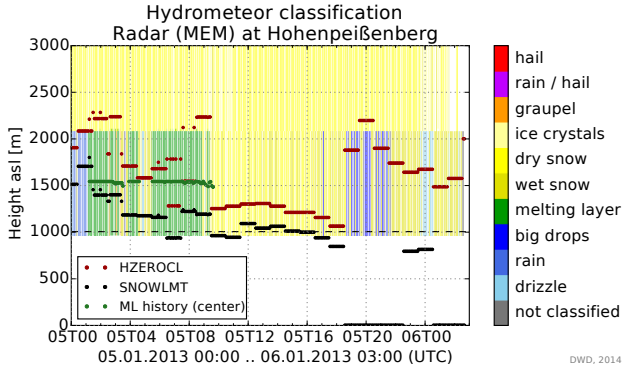
Fig. 16. Time series of the hydrometeor classification for the precipitation scan and the volume scan of radar MEM at the position of MHP. Overlaid is the $0°$C level HZEROCL (brown), the snowfall altitude SNOWLMT (black) and the center of the ML height (green). The considered time span ranges from 0:00 UTC, 05.01.2013, until 3:00 UTC, 06.01.2013. The color table for the hydrometeor classes is the same as in Figure 14.

Fig. 17. Time series of the hydrometeor classification for the 0.5 $°$ elevation volume sweep of radar MEM at the position of MHP. At this location the radar ray has a mean vertical extension of 1127 m and the height of the ray bottom is estimated with 959 m asl. Displayed are the distinct hydrometeor classes with the highest detection probability.

The color table of the hydrometeor classes is the same as in Figure 14. The melting layer can be seen until about 10:00 UTC which corresponds in timing and location quite well with melting layer height seen in Figures 6 and 7. After about 10:00 UTC, wet snow is diagnosed in the lowest layer as the most likely HM type. A closer look on the classification results is given in Figure 17. The HM classifications from the optical disdrometer are shown in Figure 18.

The $0°$C level at 12 UTC of the model (Figure 16) near 1400 m matches very well with $0°$C level from the Munich radiosonde sounding (Figure 5). We also note the increase of the $0°$C level prior 12 UTC which is consistent with the pas-

Fig. 18. Time series of the hydrometeor classification from Thies disdrometer, located at MHP. The hydrometeor classes are based on the synoptic classification related to table 4680. Mixtures of classes are denoted as combination of the distinct classes.

sage of the warm front. The Hymec result primarily shows wet snow around 12 UTC (Figure 17).

As mentioned before, a direct comparison between radar observations and a disdrometer has its limitations related to the inherently different sampling volume and sampling time. The comparison of the HM classifications based on those two sensors is further complicated since the class definitions do not match perfectly. The classification of the disdrometer (Figure 18) shows a mixture of drizzle or rain mixed with snow between 0:00 UTC and 15:00 UTC. Then predominantly snow is diagnosed which agrees well with the eye observations. The classification of the mixed rain snow class as the prime HM class until about 15:00 UTC may not match precisely the weather observer's reports. However, there are sporadic rain/drizzle observations which may be considered as a hint that rain is more predominant and that the standard HM classification of the disdrometer perhaps requires an optimization of the class definition. During the time of rain and sleet observations (based on the weather observer) until 16:45 UTC, the radar based HM detection predominantly sees dry and also some wet snow as the prime HM (Figure 17). It is consistent with what may be expected when measuring locally in a ML during an orographic rain event (recall that the depth of the ML can be on the order of several hundred meters), where, as discussed before, diabatic cooling is causing a temperature decrease so that snow may eventually reach the ground even in an initially "warm" airmass. From an operational point of view, the radar information has to be linked to the surface observations. This may be achieved through an optimization of the fuzzy logic scheme to better take into account the thermodynamic state of the atmosphere during such a weather event, i.e. by the use of thermodynamic profiles, or by a statistical correction similar to a "model output statistics" (MOS) scheme (e.g. Glahn et al. 1972). A rigorous statistical verification for many more cases

and meteorological situations is needed to validate the fuzzy logic scheme.

7   Conclusions

An orographic precipitation event on 5th/6th January 2013 is analyzed with respect to its temporal and spatial variability using polarimetric radar data. Radar data from the bird-bath scan together with disdrometer measurements at Hohenpeißenberg show the steady decrease of the melting layer in the course of the event until there is a transition into snow, which is indicated by the disdrometer measurements and confirmed by the weather observer. The Hohenpeißenberg mountain top is in the ML for several hours. Radar measurements above the melting layer shows a distinct mesoscale structure (length scale on the order of 25 km) that are interpreted as large wet snow because of the increased fall velocity on the order of 3 m/s. Associated surface observations show an increase in rain rate. This observation can be linked to the passage of a warm front. The radar measurements represent a cross section through this front when it is passing the site from north to south. Lifting processes (indicated by a drop in surface pressure), increased available moisture and forced ascent of the airmass due to the presence of orography leads to riming of snow and aggregation.

A typical feature of an orographic precipitation event is, depending on the season, the transition from rain into snow due to diabatic cooling. This is a relevant meteorological situation for a weather service, which needs to be forecasted and detected by weather observing systems. Radar systems are the only devices that can provide a look into the precipitation process in high spatial and temporal resolution. With the introduction of new polarimetric radar systems a much better characterization of the hydrometeors is now possible. "Hymec" is DWD's newly developed HM classifier which is evaluated for this precipitation event. We use the Hymec results based on the volume and precipitation scan of the Memmingen radar which is situated 65 km away from Hohenpeißenberg. The Hymec detection of the melting layer height corresponds well with the radar observations of the birdbath scan. Once the ML is just above Hohenpeißenberg the HM are classified as wet snow with sporadic pockets of large rain drops, while there is still rain observed at the surface. The model predicted $0°$C level agrees well with sounding data. Considering the size of the radar sensing volume and the fact that ML is above the radar site, the Hymec classification appears consistent with the meteorological situation, even though there is a mismatch with the in-situ observations. For this particular situation, it is expected that detailed thermodynamic input to Hymec or a statistical correction of the HM classification may help to better link the classification result to the surface observation. From an operational point of view of a weather service, this is one relevant "reference point". A thorough validation of Hymec is underway. The results shown here are promising and indicate that the principle implementation has achieved a good level of quality considering the complexity of the precipitation phenomena.

The birdbath scan, which is usually used only for calibration purposes is shown to be a valuable source of meteorological information, as it provides a high resolution view of the precipitation process and dynamics above the radar site. It can reveal the corresponding variability in time and space. In this case, a warm front associated with a trough could be detected. With the common introduction of polarimetric radars in operational weather radar networks in recent years, birdbath scans become more and more available in the operational scanning. It is suggested to not only use this scan for radar calibration purposes (which is commonly the case) but also to exploit the meteorological information available with this scan. From an operational point of view the birdbath scan fits perfectly into DWD's scan strategy where a volume scan is provided every 5 minutes. It can be viewed as an additional sweep of the volume scan.

References

Al-Sakka, H., Boumahmoud, A.-A., Fradon, B., Frasier, S. J., and Tabary, P.: A new fuzzy logic hydrometeor classification scheme applied to the French X-, C-, and S-band polarimetric radars, J. Appl. Meteor. Climatol., 52, 2328–2344, 2013.

Baldauf, M., Förstner, J., Klink, S., Reinhardt, T., Schraff, C., Seifert, A., and Stephan, K.: Kurze Beschreibung des Lokal-Modells Kürzestfrist COSMO-DE (LMK) und seiner Datenbanken auf dem Datenserver des DWD, Tech. rep., Deutscher Wetterdienst, 2014.

Bringi, V. N. and Chandrasekar, V.: Polarimetric Doppler Weather Radar, Cambridge University Press, 2001.

Fabry, F. and Zawadzki, I.: Long-term Radar Observations of the Melting Layer of Precipitation and their Interpretation, J. Atmos. Sci., 52, 838–851, 1995.

Frech, M.: Monitoring the data quality of the new polarimetric weather radar network of the German Meteorological Service, in: 36rd AMS Conf. on Radar Meteorology, Breckenridge, CO, USA, p. 16, AMS, 2013a.

Frech, M.: Observations of a mesoscale convective System, in: 36rd AMS Conf. on Radar Meteorology, Breckenridge, CO, USA, AMS, 2013b.

Frech, M., Lange, B., Mammen, T., Seltmann, J., Morehead, C., and Rowan, J.: Influence of a Radome on Antenna Performance, J. Atmos. and Oceanic Tech., 30, 313–324, 2013.

Friedrich, K., Higgins, S., Masters, F. J., and Lopez, C. R.: Articulating and Stationary PARSIVAL Disdrometer Measurements in Conditions with Strong Winds and Heavy Rainfall, J. Atmos. and Oceanic Tech., 30, 2063–2080, 2013.

Giangrande, S. E., Krause, J. M., and Ryzhkov, A. V.: Automatic designation of the melting layer with a polarimetric prototype of the WSR-88D radar, J. Appl. Meteor. Climatol., 47, 1354–1364, 2008.

Glahn, H. R. and Lowry, D. A.: The use of model output statistics (MOS) in objective weather forecasting, Journal of Applied Meteorology, 11, 1203–1211, 1972.

Houze, R. A. and Medina, S.: Turbulence as a Mechanism for Orographic Precipitation Enhancement, Journal of the Atmospheric Sciences, 62, 3599–3623, 2005.

Keenan, T.: Hydrometeor classification with a C-band polarimetric radar, Aust. Meteor. Mag, 52, 23–31, 2003.

Lackmann, G. M., Keeter, K., Lee, L. G., and Ek, M. B.: Model representation of freezing and melting precipitation: implications for winter weather forecasting, Wea. Forecasting, 17, 1016–1033, 2002.

Lim, S., Chandrasekar, V., and Bringi, V. N.: Hydrometeor classification system using dual-polarization radar measurements: Model improvements and in situ verification, Geoscience and Remote Sensing, IEEE Transactions on, 43, 792–801, 2005.

Park, H., Ryzhkov, A. V., Zrnić, D. S., and Kim, K.-E.: The hydrometeor classification algorithm for the polarimetric WSR-88D: Description and application to an MCS., Weather & Forecasting, 24, 730–748, 2009.

Rathmann, N. and Mott, M.: Effective radar algorithm software development at the DWD, in: 7th Europ. Conf. On Radar in Meteor. and Hydrol., NET316, http://www.meteo.fr/cic/meetings/2012/ERAD/extended_abs/NET_316_ext_abs.pdf, 2012.

Ryzhkov, A., Zrnic, D. S., and Gordon, B. A.: Polarimetric Method for Ice Water Content Determination, Journal of Applied Meteorology, 37, 125–134, 1998.

Ryzhkov, A., Schuur, T., Burgess, D., Heinselman, P., Giangrande, S. E., and Zrnic, D. S.: The Joint Polarization Experiment. Polarimetric Rainfall Measurements and Hydrometeor Classification, Bull. Amer. Meteorol. Soc., 86, 809 –824, 2005.

Scharfenberg, K. A., Schuur, T. J., Schlatter, P. T., Giangrande, S. E., Melnikov, V. M., Burgess, D. W., Jr., D. L. A., Foster, M. P., and Krause, J. M.: The Joint Polarization Experiment: polarimetric radar in forecasting and warning decision making, Wea. Forecasting, 20, 775–788, 2005.

Schuur, T. J., Park, H.-S., Ryzhkov, A. V., and Reeves, H. D.: Classification of precipitation types during transitional winter weather using the RUC model and polarimetric radar retrievals, J. Appl. Meteor. Climatol., 51, 763–779, 2012.

Seltmann, J. E. E., Hohmann, T., and Frech, M.: DWD's new operational scan strategy, in: 36rd AMS Conf. on Radar Meteorology, Breckenridge, CO, AMS, 2013.

Steinert, J., Werner, M., and Tracksdorf, P.: Hydrometeor classification and quantitative precipitation estimation from quality assured radar data for the DWD C-band weather radar network, 36th Conf. On Radar Meteor., 16. - 20. September 2013, Breckenridge, CO, USA, https://ams.confex.com/ams/36Radar/webprogram/Handout/Paper228477/ams2013_poster363_steinert.pdf, 2013.

Straka, J. M., Zrnić, D. S., and Ryzhkov, A. V.: Bulk hydrometeor classification and quantification using polarimetric radar data: Synthesis of relations, Journal of Applied Meteorology, 39, 1341–1372, 2000.

Szyrmer, W. and Zawadzki, I.: Snow Studies. Part II: Average Relationship between Mass of Snowflakes and Their Terminal Fall Velocity, J. Atmos. Sci., 67, 3319–3335, 2010.

Werner, M. and Steinert, J.: New quality assurance algorithms for the DWD polarimetric C-band weather radar network, in: 7th Europ. Conf. On Radar in Meteor. and Hydrol., NET403, http://www.meteo.fr/cic/meetings/2012/ERAD/extended_abs/NET_403_ext_abs.pdf, 2012.

Yuter, S. E., Kingsmill, D. E., Nance, L. B., and Löffler-Mang, M.: Observations of precipitation size and fall speed characteristics within coexisting rain and wet snow, J. Appl. Meteor. Clim., 45, 1450–1464, 2006.